Journal of Computational Physics 228 (2009) 4291–4302

Contents lists available at ScienceDirect

Journal of Computational Physics

journal homepage: www.elsevier.com/locate/jcp

Adiabatic perturbations for compactons under dissipation and numerically-induced dissipation

Francisco Rus [a], Francisco R. Villatoro [b,*]

[a] E.T.S. Ingeniería Informática, Dept. Lenguajes y Ciencias de la Computación, Universidad de Málaga, Campus de Teatinos, 29071 Málaga, Spain
[b] E.T.S. Ingenieros Industriales, Dept. Lenguajes y Ciencias de la Computación, Universidad de Málaga, Campus de El Ejido, 29013 Málaga, Spain

ARTICLE INFO

Article history:
Received 18 April 2008
Received in revised form 9 March 2009
Accepted 9 March 2009
Available online 17 March 2009

MSC:
34E10
35Q53
58J37
65M60

Keywords:
Perturbation methods
Adiabatic perturbations
Numerical methods
Compactons
Numerically-induced tails

ABSTRACT

Compacton propagation under dissipation shows amplitude damping and the generation of tails. The numerical simulation of compactons by means of dissipative schemes also show the same behaviors. The truncation error terms of a numerical method can be considered as a perturbation of the original partial differential equation and perturbation methods can be applied to its analysis. For dissipative schemes, or when artificial dissipation is added, the adiabatic perturbation method yields evolution equations for the amplitude loss in the numerical solution and the amplitude of the numerically-induced tails. In this paper, such methods are applied to the $K(2,2)$ Rosenau–Hyman equation, showing a very good agreement between perturbative and numerical results.

1. Introduction

Perturbation or asymptotic methods [1] can be used for the analysis of the errors introduced by numerical methods when the local truncation error is considered as a perturbation of the original differential equation. For the initial value problem in ordinary differential equations, regular and singular perturbation methods have been straightforwardly applied with success [2,3, and references therein]. For nonlinear evolution equations, the application of perturbation methods in such a context is more difficult, being only scarcely presented in the literature. A few exceptions require attention. Herman and Kickerbocker [4] use direct perturbations not based in the inverse scattering transform in order to study the numerically-induced phase shift in solitons of the Korteweg-de Vries equation propagated by means of the Zabusky–Kruskal scheme. Similar results have been obtained by Marchant and Smyth [5] and Marchant [6] for generalizations of, respectively, the Korteweg-de Vries and the Benjamin–Bona–Mahoney equations. Recently, Junk et al. [7] have studied by asymptotic methods the finite discrete-velocity method for the lattice Boltzmann equation, determining order-by-order the accuracy and structure of the error of the numerical equivalents for the flow velocity, pressure, and vorticity.

* Corresponding author. Tel.: +34 95 2132096; fax: +34 95 2132816.
E-mail addresses: rusman@lcc.uma.es (F. Rus), villa@lcc.uma.es (F.R. Villatoro).

0021-9991/$ - see front matter © 2009 Elsevier Inc. All rights reserved.
doi:10.1016/j.jcp.2009.03.005

The solitary wave solutions of generalized Korteweg-de Vries may have compact support, the so-called compactons, instead of presenting exponentially decreasing tails, characteristic of solitons. Let us consider the $K(2,2)$ compacton equation by Rosenau and Hyman [8], given by

$$u_t - c_0 u_x + (u^2)_x + (u^2)_{xxx} = 0, \tag{1}$$

where $u(x,t)$ is the wave amplitude, x is the spatial coordinate, t is time, c_0 is a constant velocity, and the subindex indicate differentiation. The compacton solution of Eq. (1) is given by

$$u_c(x,t) = \frac{4c}{3}\cos^2\left(\frac{x-(c-c_0)t}{4}\right), \quad |x-(c-c_0)t| \leqslant 2\pi, \tag{2}$$

where c is the velocity of the compacton.

Numerical solutions of the $K(2,2)$ equation show several numerically-induced phenomena, such as spurious radiation [9] or "artificial tails" [10]. Perturbation methods may be applied in order to understand these phenomena and to estimate their magnitudes, however, no general perturbation theory for compactons has been developed in the past. Recently, Pikovsky and Rosenau [10] have applied the method of adiabatic perturbations to compactons. This method is widely known in soliton theory [11–14], yielding the evolution of the soliton parameters on a slow time variable resulting from that of the invariants of the partial differential equation. This method is applicable only for dissipative perturbations. In Ref. [10], only second- and fourth-order linear dissipation for compactons of the $K(2,2)$ equation have been studied.

In this paper, the adiabatic perturbation method is applied to the analysis of the numerically-induced phenomena in the numerical integration of Eq. (1) by means of two numerical methods, based on either the implicit Euler or the implicit midpoint rule in time with a fourth-order spatial discretization, with and without "artificial" dissipation. Sections 2 and 2.1 present both numerical methods and representative numerical results illustrating the damping of the numerical compactons and the generation of tails. Section 3, after briefly reviewing the adiabatic perturbation method for Eq. (1), presents its application to the implicit Euler method in Section 3.1 without "artificial" dissipation and in Section 3.2 for both methods with "artificial" dissipation. In Section 4 the perturbative results are compared with those obtained by the numerical methods in order to determine their scope of validity. Section 5 is devoted to the main conclusions and future lines of research. Finally, an Appendix A detailing the derivation of some equations is included.

2. Numerical methods

Let us consider the numerical solution of the compacton Eq. (1) by means of a Petrov–Galerkin approximation in space with periodic boundary conditions, using C^0 continuous piecewise linear interpolants as trial functions and C^2 continuous Schoenberg cubic B-splines test functions. For the nonlinear terms, the product approximation is applied. The resulting weak formulation for Eq. (1) is as follows: Find a function

$$u(x,t) = \sum_{j=0}^{N} U_j(t)\phi_j(x),$$

such that

$$\langle U_t, \psi_k\rangle - c_0\langle U_x, \psi_k\rangle + \langle (U^2)_x, \psi_k\rangle + \langle (U^2)_x, (\psi_k)_{xx}\rangle = 0, \tag{3}$$

for all $\psi_k(x), k = 0,1,\ldots,N$, where a uniform mesh is used, $x_j = x_0 + j\Delta x$, the inner product is

$$\langle f, g\rangle = \int_{x_0}^{x_N} f(x)g(x)dx,$$

$U_j(t) = U(x_j,t)$ approximates $u(x_j,t)$, $\phi_j(x)$ are the usual piecewise linear hat functions associated with the node x_j ($\phi_j(x_k) = \delta_{jk}$, the Kronecker delta), and $\psi_k(x)$ are cubic B-splines defined in a $4\Delta x$ interval, which are C^2 continuous as required by Eq. (3).

The evaluation of the inner products in Eq. (3), applying the product approximation, yields the following system of ordinary differential equations

$$\mathcal{A}(\mathrm{E})\frac{dU_j}{dt} - c_0\mathcal{B}(\mathrm{E})U_j + \mathcal{B}(\mathrm{E})(U_j)^2 + \mathcal{C}(\mathrm{E})(U_j)^2 = 0, \tag{4}$$

where E is the shift operator, i.e., $\mathrm{E}U_j = U_{j+1}$ and

$$\mathcal{A}(\mathrm{E}) = \frac{\mathrm{E}^{-2} + 26\mathrm{E}^{-1} + 66 + 26\mathrm{E}^{1} + \mathrm{E}^{2}}{120},$$
$$\mathcal{B}(\mathrm{E}) = \frac{-\mathrm{E}^{-2} - 10\mathrm{E}^{-1} + 10\mathrm{E}^{1} + \mathrm{E}^{2}}{24\Delta x},$$
$$\mathcal{C}(\mathrm{E}) = \frac{-\mathrm{E}^{-2} + 2\mathrm{E}^{-1} - 2\mathrm{E}^{1} + \mathrm{E}^{2}}{2\Delta x^3}.$$

The method of lines given by Eq. (4) is fourth-order accurate for regular enough solutions since its truncation error terms are given by

$$U_t - c_0(U)_x + (U^2)_x + (U^2)_{xxx} = \frac{\Delta x^4}{240}\frac{\partial^7 U^2}{\partial x^7} + O(\Delta x^6).$$

However, in multicompacton solutions of the $K(2,2)$ equation, even for smooth initial data, shocks (or nonsmooth solutions) are developed reducing the effective order of accuracy and introducing numerical instabilities. Artificial viscosity must be introduced into the non-dissipative method given by Eq. (4) in order to avoid such instabilities. Here, as in Refs. [9,15–17] the term $\mu\partial^4 u/\partial x^4$, with small positive μ, is introduced into the left-hand side of Eq. (1). This term is numerically discretized by means of a second-order accurate five-point difference formula, given by

$$\mathcal{D}(\mathrm{E})U_j = \frac{\mathrm{E}^{-2} - 4\mathrm{E}^{-1} + 6 - 4\mathrm{E}^{1} + \mathrm{E}^{2}}{\Delta x^4}U_j, \tag{5}$$

which is added to the left-hand side of Eq. (4).

Let us consider two methods for the integration in time of Eq. (4):

Method 1. The first-order implicit Euler method given by

$$\mathcal{A}(\mathrm{E})\frac{U_{j,m+1} - U_{j,m}}{\Delta t} - (c_0\mathcal{B}(\mathrm{E}) - \mu\mathcal{D}(\mathrm{E}))U_{j,m+1} + (\mathcal{B}(\mathrm{E}) + \mathcal{C}(\mathrm{E}))(U_{j,m+1})^2 = 0,$$

where $U_{j,m} \approx u(x_j, t_m)$, and $t_m = m\Delta t$.

Method 2. The second-order implicit midpoint rule, which is written as

$$\mathcal{A}(\mathrm{E})\frac{U_{j,m+1} - U_{j,m}}{\Delta t} - (c_0\mathcal{B}(\mathrm{E}) - \mu\mathcal{D}(\mathrm{E}))\left(\frac{U_{j,m+1} + U_{j,m}}{2}\right) + (\mathcal{B}(\mathrm{E}) + \mathcal{C}(\mathrm{E}))\left(\frac{U_{j,m+1} + U_{j,m}}{2}\right)^2 = 0.$$

Methods 1 and 2 are of first- and second-order, respectively, of accuracy in time. The linear stability analysis by using the von Neumann method for Methods 1 and 2, after linearization of Eq. (1), i.e., by taking $u^2 = Uu$, with $U = 2(\|u\|_\infty)$, shows that Method 1 is L-stable and Method 2 is A-stable, see Refs. [16,17]. Hence, both methods are (linearly) unconditionally stable.

2.1. Numerical propagation of compactons

Let us consider the numerical simulation of the propagation of a compacton by means of Methods 1 and 2, for $\mu = 0$. Fig. 1 (left plot) shows a comparison between the compacton solution propagated by Method 1 (continuous line) and Method 2 (dashed line). Method 1 is dissipative for $c_0 \neq c$, hence the amplitude of the numerical compacton propagated by this method decreases with time, but Method 2 is non-dissipative and its results do not show any visible damping, as illustrated in Fig. 1 (left plot).

Extensive numerical results show that the numerical compacton propagated by means of Method 1 for $c_0 \neq c$, shows a "tail" which stretches from its left edge at $t = 0$, but no tail is found for either $c_0 = c$ or when Method 2 is used. A typical tail profile is illustrated in Fig. 1 (right plot), obtained by means of a vertical zoom of the result shown in Fig. 1 (left plot), where the small tail is not appreciable. Note that the amplitude of the tail, after reaching a local maximum, decreases monotonically to zero, hence in long-time simulations the tail decouples from the compacton, presenting a finite length (not illustrated in Fig. 1).

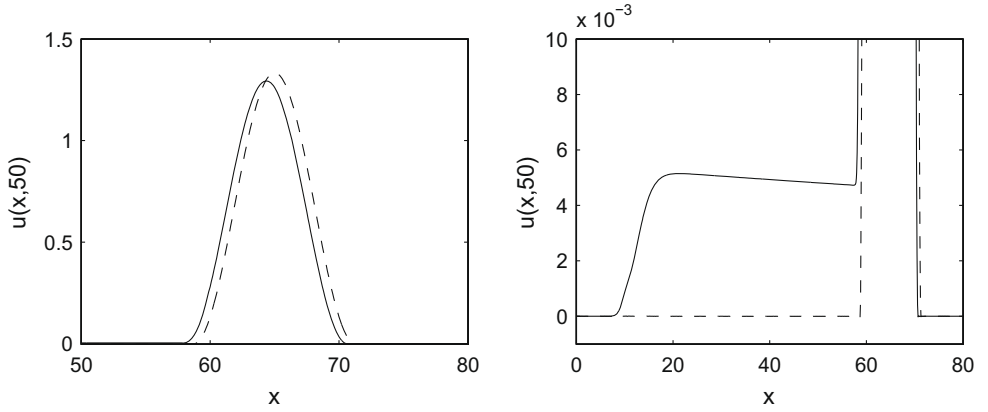

Fig. 1. Numerical solutions at $t = 50$ obtained by means of Methods 1 (continuous line) and 2 (dashed line) for a one compacton solution with $\Delta t = 0.05, \Delta x = 0.1, c_0 = 1/2, c = 1$, and $\mu = 0$. The right plot shows a vertical zoom of the result shown in the left plot.

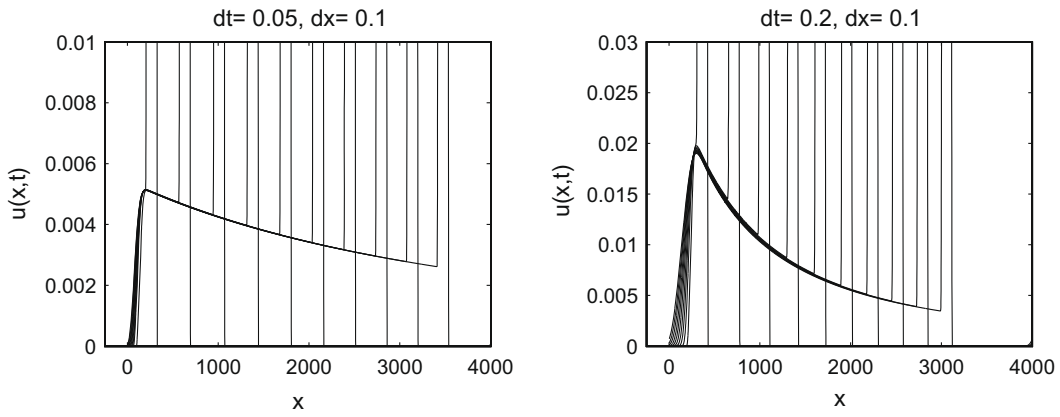

Fig. 2. Superposition of multiple numerical solutions obtained at times $t = 10, 50, 90, 130, 170, 210, 250, 290, 330$, and 370, such that the point at which the tail has a local maximum coincides among them, by using Method 1 for $\Delta t = 0.05$ (left plot) and $\Delta t = 0.2$ (right plot), both with $\Delta x = 0.1, c = 1, c_0 = 1/2$, and $\mu = 0$.

Numerical simulations show that the shape of the compacton tail due to the use of Method 1 has a profile that does not change appreciably during the propagation of the compacton, as illustrated in Fig. 2, where the profile of the tail is clearly visible by means of plotting several numerical results at different times superposed in such a way that the position of the local maximum of the corresponding tails coincides. Fig. 2 shows that the slope of the front of the tail and the amplitude of its local maximum decrease slowly in time.

In long time integrations using Method 1 under periodic boundary conditions, the tail of the compacton reenters the domain several times, mounting over itself, as illustrated in Fig. 3 for the intervals of integration [0, 80] (left plot) and [0, 150] (right plot). In order to illustrate such behavior, both plots in Fig. 3 show a superposition of the numerical solutions at different times such that the position of the compactons have been reallocated in order to coincide exactly. The slope of the front of the tail decreases, but its amplitude increases, as the tail reenters the domain several times. The finiteness of the length of the tail results in a diminishing of the increment in amplitude of the tail after each reentering, as shown in both plots of Fig. 3.

Numerical simulations of the propagation of a compacton by means of Methods 1 and 2, for $\mu > 0$, show the appearance of a dissipative tail, illustrated in, respectively, the left plot and the right one of Fig. 4, both for μ = 0.1, 0.01, and 0.001. Fig. 4 (left plot), corresponding to Method 1, shows that the amplitude of the tail diminishes as μ does until reaching the amplitude of the tail for $\mu = 0$, which coincides with that of $\mu = 0.001$ up to the plot resolution. Such behavior does not appear in Method 2, shown in Fig. 4 (right plot), for which the tail disappears as μ diminishes. For large μ, both plots in Fig. 4 show that the tail presents a peak in its left front, and Fig. 4 (left plot) shows that the tail has a finite slope which is not visible in Fig. 4 (right plot), where a nearly constant positive plateau can be observed (in fact, longer simulations show that the tail also has a small negative slope). The results shown in both plots in Fig. 4 suggest that the tails of Methods 1 and 2 have a finite length and that those of Method 1 are the addition of two independent tails whose front velocity is the same but differs in amplitude.

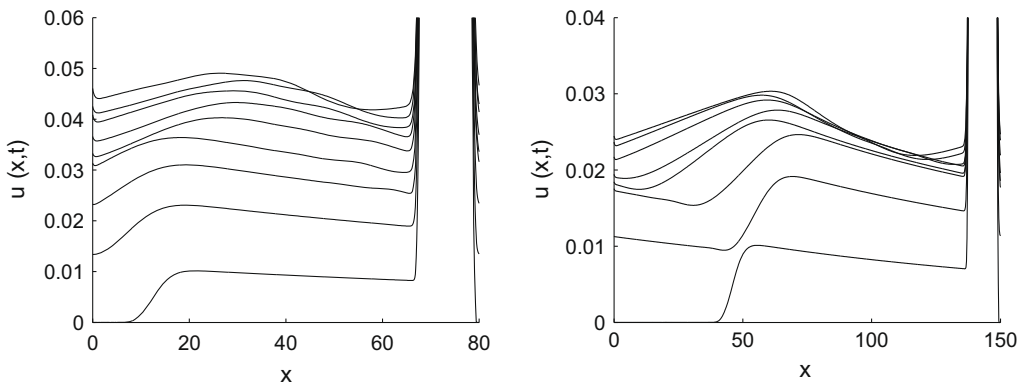

Fig. 3. Superposition of multiple numerical solutions under periodic boundary conditions such that the point at which the compacton has a maximum coincides among them, for an interval of integration of [0, 80] (left plot) and [0, 150] (right plot) by using Method 1 for $\Delta t = 0.1, \Delta x = 0.1, c = 1, c_0 = 1/2$, and $\mu = 0$. Left plot shows solutions at times $t = 60, 240, 440, 660, 880, 1120, 1380, 1640$, and 1920, and right plot at times $t = 100, 450, 1100, 1600, 2100, 2900, 3450$, and 4000, in both cases corresponding to tails from bottom to top.

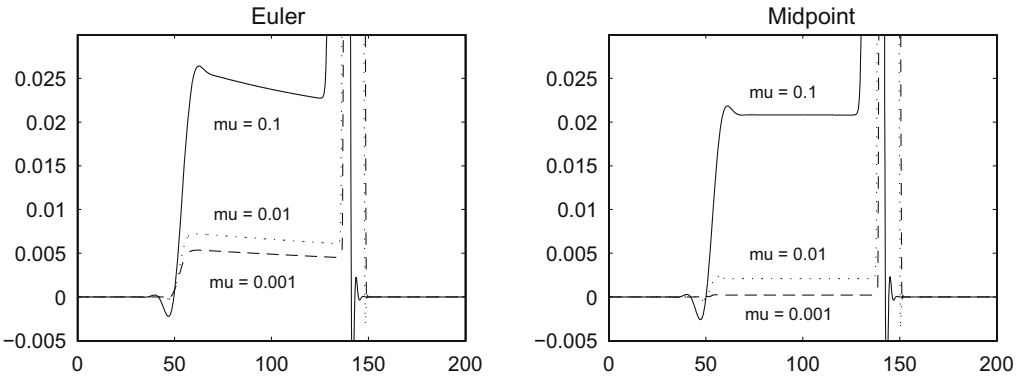

Fig. 4. Zooms highlighting the tail for a numerical compacton propagated with Method 1 (left plot) and Method 2 (right plot) for $\mu = 0.1$ (continuous line), 0.01 (dotted line), and 0.001 (dashed line), where $\Delta t = 0.05, \Delta x = 0.1, c = 1$, and $c_0 = 1/2$.

3. Adiabatic perturbation theory for compactons

Adiabatic perturbation theory is a technique for the analysis of solitary wave solutions of nonlinear evolution equations under dissipative perturbations. This technique determines the slow time evolution of the parameters of the solitary wave based on that of the invariants under the perturbation. It has been previously applied to solitons [11–14], and recently extended to compactons by Pikovsky and Rosenau [10]. Let us review the application of such technique to Eq. (1), whose four invariants are $I_i = \int \phi_i(u)dx$, where $\phi_1 = u, \phi_2 = u^3, \phi_3 = u\cos(x)$, and $\phi_4 = u\sin(x)$.

Let us consider a perturbation of the $K(2,2)$ Eq. (1) given by

$$u_t + (u^2)_x + (u^2)_{xxx} - c_0 u_x = \mathcal{P}(u), \tag{6}$$

where $|\mathcal{P}(u)| \ll 1$ is a small function of u and its spatial and temporal derivatives. The integration in space of Eq. (6) yields

$$\frac{d}{dt}\int_{-\infty}^{\infty} u\,dx = \int_{-\infty}^{\infty} \mathcal{P}(u)dx, \tag{7}$$

where the left-hand side is the temporal derivative of the first invariant of Eq. (1), i.e., exactly nil, and the right-hand side can be null for perturbations preserving the first invariant (for example, for $\mathcal{P}(u) = \partial\mathcal{Q}(u)/\partial x$), otherwise being non-zero.

Eq. (7) may be used to determine the adiabatic evolution of the parameters of the compacton solution of the $K(2,2)$ equation if the perturbation does not preserve the first invariant. In such a case, an ansatz for a perturbed compacton solution of Eq. (6), given by

$$u_c(x,t) = \frac{4c(t)}{3}\cos^2\left(\frac{x-(c(t)-c_0)t}{4}\right), \quad |x-(c(t)-c_0)t| \leqslant 2\pi, \tag{8}$$

can be introduced into Eq. (7) yielding a differential equation for $c(t)$, from which the adiabatic evolution due to the perturbation of the velocity and amplitude $(4c(t)/3)$ of the compacton can be determined. Note that, for an adiabatic perturbation, $c(t)$ must be a slowly varying function of the time, usually, depending on a small parameter characterizing the smallness of the perturbation. As an example, let us take $\mathcal{P}(u) = -\varepsilon u$, with $|\varepsilon| \ll 1$, for which Eq. (7) for u_c given in Eq. (8) yields

$$\frac{8\pi}{3}\frac{dc(t)}{dt} = -\varepsilon\frac{8\pi}{3}c(t),$$

whose solution is

$$c(t) = c(0)e^{-\varepsilon t},$$

indicating that both the amplitude and the velocity of the compacton decrease slowly as it evolves in time.

The adiabatic evolution of the parameters of the compacton for perturbations preserving the first invariant but not preserving the second one, can be studied by similar means. Multiplying Eq. (6) by u^2 and integrating in space results in

$$\frac{d}{dt}\int_{-\infty}^{\infty}\frac{u^3}{3}dx = \int_{-\infty}^{\infty} u^2\mathcal{P}(u)\,dx, \quad \int_{-\infty}^{\infty}\mathcal{P}(u)\,dx = 0, \tag{9}$$

where the substitution of the compacton ansatz (8) gives an ordinary differential equation for the velocity $c(t)$ as function of the slow time t.

Pikovsky and Rosenau [10] have considered only the perturbation $\mathcal{P}(u) = \alpha u_{xx} - \beta u_{xxxx}$, with $|\alpha|, |\beta| \ll 1$, which preserves the first invariant, for which Eq. (9) is

$$\frac{80\pi}{27}c^2(t)\frac{dc(t)}{dt} = -\frac{2\pi}{27}(4\alpha+\beta)c^3(t),$$

whose solution is

$$c(t) = c(0)e^{-(4\alpha+\beta)t/40}.$$

For a dissipative perturbation ($\alpha, \beta > 0$) both the velocity and amplitude of the perturbed compacton diminish slowly in time.

3.1. Adiabatic perturbations for numerically-induced dissipation

The truncation error terms in the modified equation of a numerical method [2,18] may be interpreted as a numerically-induced perturbation to the original equation which can be analyzed by means of using asymptotic or perturbation methods [4]. Such an approach can be applied to compactons numerically propagated by Methods 1 and 2, unfortunately, a general perturbation method for compactons has not been developed yet. The adiabatic perturbation method for compactons may be applied, at least, for dissipative numerical methods, like Method 1.

Method 1 preserves the first invariant of Eq. (1), hence Eq. (9) can be used to determine the evolution of the parameters of a numerically perturbed compacton as function of the grid size and the time step, when the perturbation $\mathcal{P}(u)$ corresponds to its truncation error terms. For Method 1, the corresponding perturbation is [19,20]

$$\mathcal{P}_1(u) = -\mathcal{A}(\mathrm{E})\frac{u(x,t+\Delta t)-u(x,t)}{\Delta t} + c_0\mathcal{B}(\mathrm{E})u(x,t+\Delta t) - (\mathcal{B}(\mathrm{E})+\mathcal{C}(\mathrm{E}))u^2(x,t+\Delta t), \tag{10}$$

where $Eu(x,t) = u(x+\Delta x,t)$ and $u(x,t)$ is a solution of Eq. (1). The evaluation of Eq. (9) for the compacton solution (8) and perturbation (10) is straightforward but cumbersome. The calculation greatly simplifies if $\mathcal{P}_1(u)$ is Taylor expanded about $t-\Delta t$, i.e., by taking

$$\mathcal{P}_1(u) = -\mathcal{A}(\mathrm{E})\frac{u(x,t)-u(x,t-\Delta t)}{\Delta t} + c_0\mathcal{B}(\mathrm{E})u(x,t) - (\mathcal{B}(\mathrm{E})+\mathcal{C}(\mathrm{E}))u^2(x,t). \tag{11}$$

The evaluation of Eq. (9) for the compacton solution (8) and perturbation (11), as detailed in Appendix A, yields

$$\frac{dc(t)}{dt} = \frac{-c(t)}{75\Delta t}\left(33+26\cos\left(\frac{\Delta x}{2}\right)+\cos(\Delta x)\right)\sin^2\left(\frac{(c_0-c(t))\Delta t}{4}\right). \tag{12}$$

The analytical solution of Eq. (12) can be obtained in implicit form, omitted here for brevity, although a numerical solution may be preferred in practice.

Eq. (11) can be simplified using its continuum limit by applying Taylor series expansion for small Δt and Δx, resulting in

$$\mathcal{P}_1(u) = \frac{\Delta t}{2}u_{tt} + \frac{\Delta x^4}{240}\frac{\partial^7 u^2}{\partial x^7} - \frac{\Delta t^2}{6}u_{ttt} + \frac{\Delta t\Delta x^2}{8}u_{xxtt} + O(\Delta t^3, \Delta t^2\Delta x^2, \Delta t\Delta x^4, \Delta x^4). \tag{13}$$

The evaluation of Eq. (9) using Eq. (13) yields

$$\frac{dc(t)}{dt} = \frac{\Delta t}{320}(\Delta x^2 - 16)(c(t)-c_0)^2c(t) + O(\Delta t^3, \Delta t\Delta x^4), \tag{14}$$

which coincides, as expected, with the corresponding Taylor series expansion of Eq. (12) up to this order. The analytical solution of Eq. (14) up to the leading order term can be easily obtained in implicit form, but omitted here for the sake of brevity.

Eqs. (12) and (14) show that in the case of $c_0 = c(0)$, there is no damping and its amplitude remains constant. This favorable behavior does not occur in multicompacton initial solutions with compactons of different velocities. In such a case, the best value for c_0, in order to minimize the damping in the compactons, has to be equal to the mean of all the compacton velocities.

A dynamical analysis of Eq. (12) shows that its steady states are $c(t) = 0$ and $c(t) = c_k = c_0 + 8\pi k/\Delta t$, for $k \in \mathbb{Z}$, being linearly and marginally stable, respectively. The steady states with $k \neq 0$ cannot be reached by the numerical method since the Courant–Friedrichs–Lewy (CFL) condition [21], which in our case yields $\Delta x/\Delta t \geqslant |c_k - c_0|$, requires $\Delta x \geqslant 8\pi|k|$, which is larger than the fixed width of any compacton for $k \neq 0$. The only steady states of Eq. (12) numerically reachable coincide with those of Eq. (14).

The qualitative behavior of the numerical solution of Eqs. (12) and (14) is the same. Let us first consider the case $c_0 > 0$. For $c(0) > c_0$, the solution $c(t)$ tends to c_0 as time goes to infinity, hence the damping rate of the compacton decreases to zero and the compacton stops (in the inertial frame moving at c_0). The amplitude of compactons with $0 < c(0) < c_0$ and anticompactons ($c(0) < 0$) diminishes to zero with time, i.e., such solutions tend to vanish. In multicompacton solutions, all the compactons with $c_i(0) > c_0$ tends to reach the same amplitude stopping at different locations, and those with $c_i(0) < c_0$ tend to disappear. For the case $c_0 < 0$, the anticompactons with $c(0) < c_0$ tends to stop in the inertial frame moving at c_0, and anticompactons with $c_0 < c(0) < 0$ and compactons ($c(0) > 0$) tend to vanish.

Method 2 also preserves the first invariant of Eq. (1), but does not conserve the second one. However, being a non-dissipative method (for $\mu = 0$), Eq. (9) cannot be used to determine the slow time evolution of $c(t)$. The proof is easy by means of considering as perturbation its truncation error terms Taylor expanded at $t + \Delta t/2$, given by

$$\mathcal{P}_2(u) = -\mathcal{A}(\mathrm{E})\frac{u(x,t+\Delta t/2) - u(x,t-\Delta t/2)}{\Delta t} + c_0\mathcal{B}(\mathrm{E})\frac{u(x,t+\Delta t/2) + u(x,t-\Delta t/2)}{2} - (\mathcal{B}(\mathrm{E}) + \mathcal{C}(\mathrm{E}))\left(\frac{u(x,t+\Delta t/2) + u(x,t-\Delta t/2)}{2}\right)^2, \tag{15}$$

for which the evaluation of Eq. (9) for the compacton solution (8) yields exactly a null value, as shown in Appendix A. This result is expected from the fact that a non-dissipative perturbation does not behave adiabatically as required by the adiabatic perturbation method [12,13].

The adiabatic perturbation method allows the estimation of the area under the tail, as shown by Pikovsky and Rosenau [10], due to the conservation of the first invariant by the perturbation. Let us assume that the solution shown in Fig. 1 (right plot) is $u(x,t) = u_c(x,t) + u_T(x,t)$, where $u_T(x,t)$ is the amplitude of the tail. The numerical simulations show that the tail stretches from the left edge of the compacton at $t = 0$, let say x_L, up to the left edge of the compacton at $t > 0$, i.e., the tail's support is $x \in [x_L, X(t)]$ where

$$X(t) = x_L + \int_0^t (c(\tau) - c_0)d\tau. \tag{16}$$

The constant value for the first invariant is given by

$$I_1 = \int_{-\infty}^{\infty} u(x,t)\,dx = \int_{X(t)}^{X(t)+4\pi} u_c(x,t)\,dx + \int_{x_L}^{X(t)} u_T(x,t)\,dx = \frac{8\pi}{3}c(t) + A_T(t), \tag{17}$$

where $A_T(t)$ is area under the tail. This expression yields

$$A_T(t) = -\frac{8\pi}{3}(c(t) - c(0)), \tag{18}$$

where $c(t)$ is the solution of Eq. (12).

In the general case, the adiabatic perturbation method cannot be used to estimate the shape of the tail. However, the point of contact between the tail and the compacton can be easily obtained from Eq. (17) as

$$u_T(X(t),t) = \frac{dA_T(t)}{dt} = -\frac{8\pi}{3}\frac{dc(t)}{dt}. \tag{19}$$

This expression can be used to estimate the shape of the tail since, as illustrated in Fig. 2 for Method 1, its profile does not change appreciably during the propagation of the compacton.

3.2. Adiabatic perturbations for artificial dissipation

The addition of artificial dissipation by a fourth-order linear term like Eq. (5) into Methods 1 and 2 introduces errors in the amplitude and velocity of the numerically propagated compactons and the presence of an "artificial tail". For Method 1, these phenomena adds to those shown in Section 3.1. Let us show how the adiabatic perturbation method can be used in order to understand the effects of Eq. (5) into Methods 1 and 2.

The perturbation introduced by Eq. (5) into Method 1 is the sum of $\mathcal{P}_1(u)$, given by Eq. (11), and $\mathcal{P}_3(u) = -\mu\mathcal{D}(\mathrm{E})u(x,t)$. The result of evaluating Eq. (9) for such perturbation yields

$$\frac{dc(t)}{dt} = -\frac{c(t)}{75\Delta t}\left(33 + 26\cos\left(\frac{\Delta x}{2}\right) + \cos(\Delta x)\right)\sin^2\left(\frac{(c_0 - c(t))\Delta t}{4}\right) - \frac{32\mu}{5\Delta x^4}\sin^4\left(\frac{\Delta x}{4}\right)c(t). \tag{20}$$

The only real steady state of Eq. (20) numerically reachable (for $\Delta x < 4\pi$) is $c(t) = 0$. Hence, both compactons and anticompactons, independently of $c(0)$, tend to disappear as time increases.

The perturbation introduced by Eq. (5) into Method 2, since $\mathcal{P}_2(u)$ has no contribution, is

$$\mathcal{P}_4(u) = -\mu\mathcal{D}(\mathrm{E})\frac{u(x,t+\Delta t/2) + u(x,t-\Delta t/2)}{2},$$

for which Eq. (9) yields

$$\frac{dc(t)}{dt} = -\frac{32\mu}{5\Delta x^4}\cos^2\left(\frac{\Delta t}{4}(c_0 - c(t))\right)\sin^4\left(\frac{\Delta x}{4}\right)c(t). \tag{21}$$

This equation can be easily solved numerically. The Taylor series expansion of Eq. (21) for small Δt results in

$$\frac{dc(t)}{dt} = -\frac{32\mu}{5\Delta x^4}\sin^4\left(\frac{\Delta x}{4}\right)c(t) + O(\Delta t^2), \tag{22}$$

whose analytical solution is

$$c(t) = e^{-\gamma t} c(0) + O(\Delta t^2),$$

where

$$\gamma = \frac{32\mu}{5\Delta x^4} \sin^4\left(\frac{\Delta x}{4}\right) = \mu\left(\frac{1}{40} - \frac{\Delta x^2}{960} + O(\Delta x^4)\right),$$

showing that the main effect of the artificial dissipation in the compactons propagated by Method 2 is an exponential damping in time of their amplitude whose rate is a function of μ, independently of Δt and Δx at the leading order of approximation. In fact, the only steady state of Eq. (21) numerically reachable (for $\Delta x < 2\pi$) is $c(t) = 0$, which is linearly stable. Hence, as with Method 1, both compactons and anticompactons tend to disappear as time increases.

Eqs. (18) and (19) can be used to estimate the area under the tail and its shape, respectively, by means of using Eq. (20) (for Method 1) and (21) (for Method 2) as a function of $\mu > 0$.

4. Presentation of results

Let us compare the numerical results of Methods 1 and 2 for the propagation of one compacton with those obtained by the adiabatic perturbation method developed in this paper in order to determine its scope of validity.

Fig. 5 (left plot) shows a comparison between the amplitude $(4c(t)/3)$ of the compacton numerically obtained by means of using Method 1 with $\mu = 0$ and the numerical evaluation of the solution of Eqs. (12) and (14), both by using an adaptive-step solver, as a function of time for $\Delta t = 0.2$ and $\Delta t = 0.05$. Extensive simulations show results similar to those presented in Fig. 5 (left plot) when the CFL condition holds, i.e., $\Delta x/\Delta t \geqslant c(t) - c_0$. Both plots in Fig. 5 (left plot) show very good agreement between numerical and perturbative results, confirming the validity of the adiabatic perturbation method. Moreover, the solutions of Eqs. (12) and (14) are indistinguishable in both plots (their difference is smaller than 10^{-6}). Our results imply that, in practice, Eq. (14) may be preferred to Eq. (12) in order to estimate the damping of the compacton solution of Method 1 for small Δt and Δx.

Fig. 5 (right plot) shows the area under the tail of a compacton propagated by Method 1 with $\mu = 0$, numerically calculated by means of the trapezoidal quadrature rule (continuous curve) and by means of the numerical evaluation of Eq. (18) (dashed curve) as function of time for $\Delta t = 0.2$ and $\Delta t = 0.05$. Both plots in Fig. 5 (right plot) show very good agreement between numerical and perturbative results. Moreover, the result of using Eq. (14) instead of Eq. (12) in the tail area estimation is indistinguishable when plotted in Fig. 5 (right plot). Similar results have been obtained for other set of parameters (when the CFL condition holds) in our extensive set of simulations (omitted here for the sake of brevity).

Fig. 6 shows the comparison between the tail shape profile obtained by means of Eq. (19) (continuous curve) and the numerical solution of Method 1 (dashed curve), for $\mu = 0$ and $\Delta t = 0.05$ (left plot) and $\Delta t = 0.2$ (right plot). Both plots in Fig. 6 show reasonable agreement between the numerical and the perturbative results for the shape of the tail between its maximum and the contacting point with the compacton. The front profile of the tail and its evolution, as shown in Fig. 2 cannot be obtained by the present adiabatic perturbation method. In fact, Eq. (12) implies that $u_T(X(0), 0)$ is non-null, since $dc(0)/dt \neq 0$ for $c(0) \neq 0$, in contradiction with the results shown in Figs. 2 and 6.

Fig. 7 shows a comparison between the numerical amplitude of the compacton obtained by means of using Method 1 (left plot) and Method 2 (right plot) with several values of μ, and the numerical evaluation of the solution of Eq. (20) (left plot)

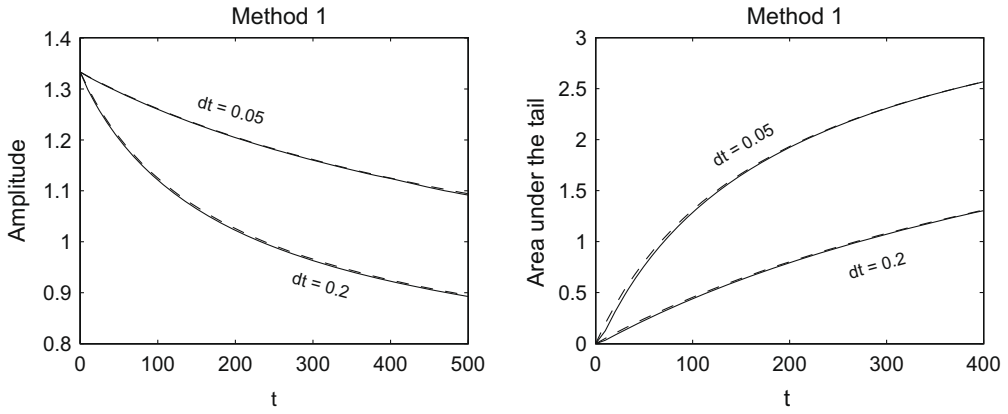

Fig. 5. Left plot: temporal evolution of the amplitude of the numerical compacton calculated with Method 1 (continuous line) and by means of Eq. (12) (dashed line). Right plot: temporal evolution of the area under the tail of a compacton propagated by means of Method 1 determined by numerical quadrature (continuous line) and by numerical evaluation of Eq. (18) (dashed line). Both plots present results for $\Delta t = 0.05$ and 0.2, with $\Delta x = 0.1, c = 1, c_0 = 1/2$, and $\mu = 0$.

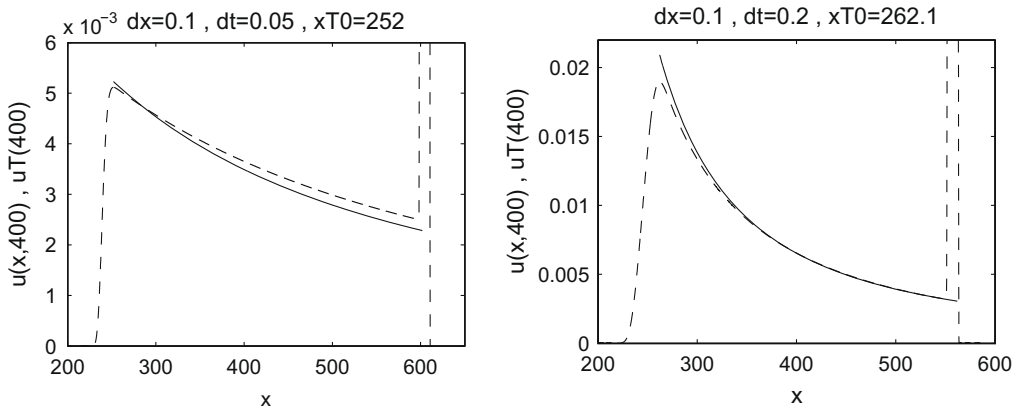

Fig. 6. Tail shape (dashed line) and its approximation (continuous line) for a numerical compacton calculated with Method 1 for $\Delta t = 0.05$ (left plot) and $\Delta t = 0.2$ (right plot) with $\Delta x = 0.1, c = 1, c_0 = 1/2$, and $\mu = 0$.

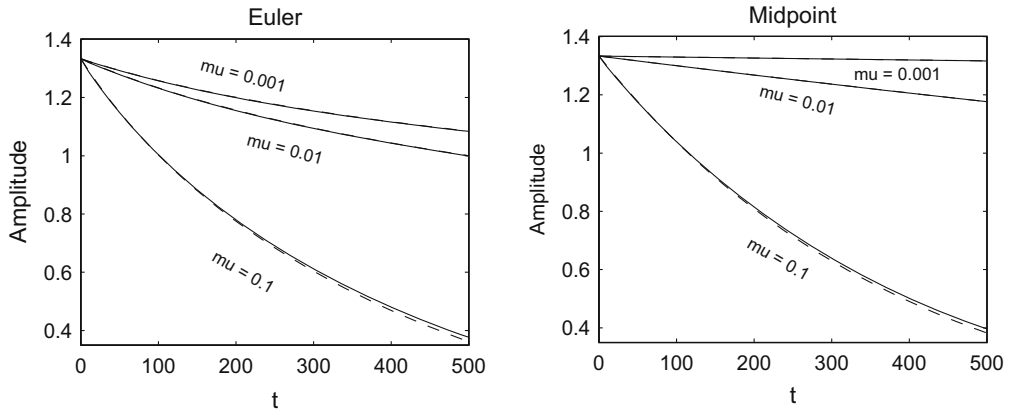

Fig. 7. Temporal evolution of the amplitude of the numerical compacton calculated by means of Eq. (20) (left plot, dashed lines) and (21) (right plot, dashed lines), and by using Method 1 (left plot, continuous lines) and Method 2 (right plot, continuous lines) for $\mu = 0.1$, 0.01, and 0.001 (as indicated in the plots), with $\Delta t = 0.05, \Delta x = 0.1, c = 1$, and $c_0 = 1/2$.

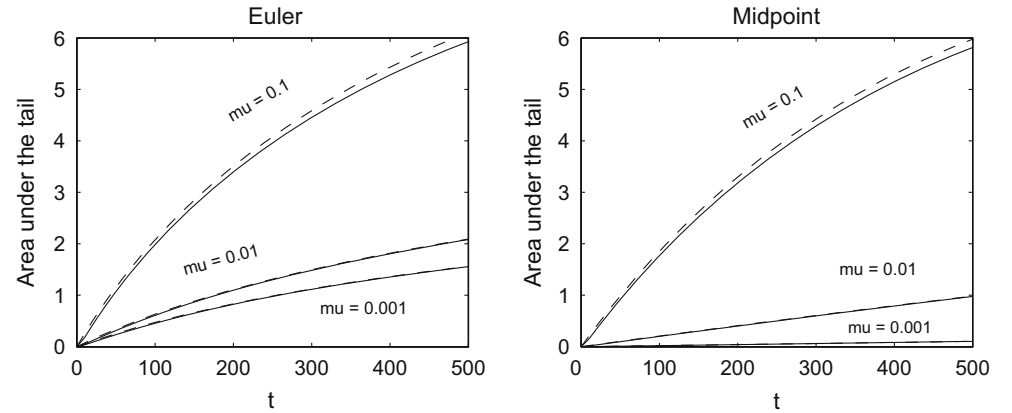

Fig. 8. Temporal evolution of the area under the tail of a compacton calculated by means of Eq. (20) (left plot, dashed lines) and (21) (right plot, dashed lines), and by using numerical quadrature applied to the solution obtained by Method 1 (left plot, continuous lines) and Method 2 (right plot, continuous lines) for $\mu = 0.1$, 0.01, and 0.001 (as indicated in the plots), with $\Delta t = 0.05, \Delta x = 0.1, c = 1$, and $c_0 = 1/2$.

and (21) (right plot). The agreement between the adiabatic perturbation results and the numerical ones is excellent for all values of μ and improves as μ decreases, verifying the validity of the asymptotic results.

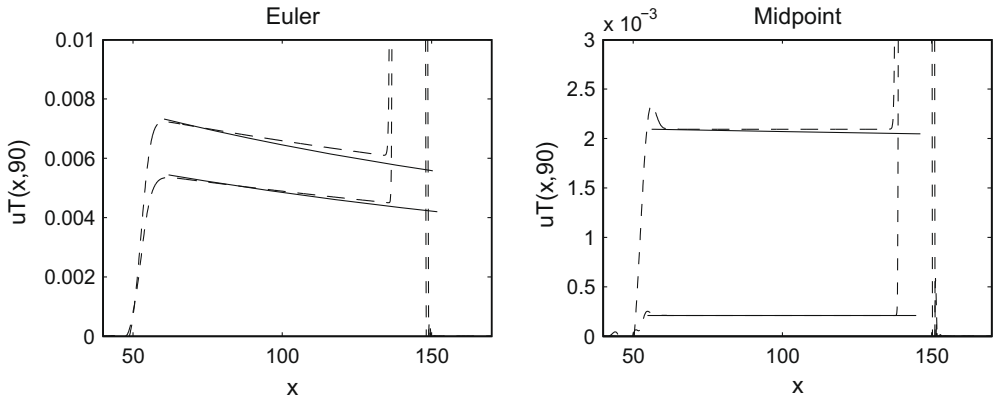

Fig. 9. Tail shapes (dashed line) and its approximations (continuous line) for a numerical compacton calculated with Methods 1 (left plot) and 2 (right plot) for $\mu = 0.01$ and 0.001, with $\Delta t = 0.05, \Delta x = 0.1, c = 1$, and $c_0 = 1/2$.

Fig. 8 shows a comparison between the numerically calculated area under the tail of the compacton obtained using Method 1 (left plot) and Method 2 (right plot) with three values of μ, and the substitution in Eq. (18) of the numerical evaluation of the solution of Eq. (20) (left plot) and (21) (right plot). Fig. 8 also verifies the validity of adiabatic perturbation method, showing the good agreement between the adiabatic perturbation results and the numerical ones, and its improvement as μ diminishes.

Fig. 9 shows the comparison between the tail shape profile obtained by means of Eq. (19) (continuous curves) and the numerical solutions (dashed curve) for Methods 1 (left plot) and 2 (right plot) with two values of μ. Both plots in Fig. 9 show good agreement between the numerical and the perturbative result for the shape of the plateau of the tail. However, the front profile of the tail cannot be estimated by the present method. Let us note that, for Method 1, Eq. (20) confirms that the tail is the result of the addition of two terms, one for $\mu = 0$ and another one depending on μ, as shown in Fig. 4 (left plot) and discussed in Section 2.1.

5. Conclusions

The adiabatic perturbation method for compactons has been applied to the analysis of the numerically-induced phenomena in two numerical methods for the $K(2,2)$ Rosenau–Hyman equation by taking into account the truncation error terms of the numerical scheme as a perturbation of the original partial differential equation. Both methods use a Petrov–Galerkin finite element formulation in space, but Method 1 uses the implicit Euler scheme in time, and Method 2 uses the implicit midpoint rule. In absence of artificial dissipation, the perturbation results for Method 1 yields equations for the adiabatic evolution of the amplitude of the compacton, the area under the numerically-generated tail, and the shape of this tail except at its front, in very good agreement with the numerical simulations. Method 2 does not show these phenomena and correspondingly the perturbation results are null. The addition of artificial dissipation in Methods 1 and 2 results in the appearance of tails and compacton amplitude loss. The adiabatic perturbation results, for both Method 1 and 2, for the evolution of the amplitude and velocity of the compacton, and the area and shape of the corresponding tails, with the exception of its front, are also in good agreement with the numerical simulations.

The approximate analytical results obtained in this paper contain very useful information on the behavior of Methods 1 and 2. For example, for Method 1 with $\mu = 0$ and $c_0 > 0$, the velocity $c(t)$ of compactons with $c(0) > c_0$, tends to c_0 as time goes to infinity, but of those with $c(0) < c_0$ tends to zero. This unexpected behavior has not been reported previously in the literature on the application of the Euler implicit method for nonlinear evolution equations, up to the authors' knowledge. For both Method 1 and 2 with $\mu > 0$, the velocity and amplitude of the compactons always decreases as time evolves. Another interesting feature discovered by our perturbation analysis is the fact that the "artifical" tails have a finite negative slope and hence a finite length.

Present results depend strongly on the dissipation of the numerical methods considered, a requirement for the application of the adiabatic perturbation method. The development of a general theory of perturbation for compactons, which may allow the analytical determination of the whole profile of the tails of the compactons, including their front shape and its evolution, is a very interesting topic for further research.

Acknowledgments

The authors acknowledge the remarks and suggestions of two anonymous reviewers which have greatly improved the contents and presentation of this paper. The research reported in this paper was partially supported by Project FIS2005-03191 from the Ministerio de Educación y Ciencia, Spain.

Appendix A. Evaluation of Eq. (9) for $\mathcal{P}_1$ and $\mathcal{P}_2$

In order to simplify the calculation, let us take $z = x - (c - c_0)t$ such that the compacton solution (8) yields

$$u_c(x,t) \equiv u_c(z) = \frac{4c}{3}\cos^2\left(\frac{z}{4}\right) = \frac{2c}{3}\left(1 + \cos\left(\frac{z}{2}\right)\right), \quad |z| \leqslant 2\pi,$$

with $u_c(z) = 0$ for $|z| > 2\pi$, and the integral in the right-hand side of Eq. (9) is given by

$$\int_{-\infty}^{\infty} u_c(x,t)^2\,\mathcal{P}(u_c(x,t))\,dx = \int_{-2\pi}^{2\pi} u_c(z)^2\,\mathcal{P}(u_c(z))\,dz. \tag{23}$$

In order to evaluate this expression for Eq. (11), let us recall that, formally, $E = \exp(\Delta x D)$ with $Du(x,t) = u_x(x,t)$ (see Ref. [20] for further details), thus the operators $\mathcal{A}(\mathrm{E}), \mathcal{B}(\mathrm{E})$ and $\mathcal{C}(\mathrm{E})$ can be written as

$$\mathcal{A}(\mathrm{E}) = \mathcal{A}(\exp(\Delta x D)) = \frac{33 + 26\cosh(\Delta x D) + \cosh(2\,\Delta x D)}{60},$$
$$\mathcal{B}(\mathrm{E}) = \mathcal{B}(\exp(\Delta x D)) = \frac{10\sinh(\Delta x D) + \sinh(2\,\Delta x D)}{12\,\Delta x},$$
$$\mathcal{C}(\mathrm{E}) = \mathcal{C}(\exp(\Delta x D)) = \frac{\sinh(2\,\Delta x D) - 2\sinh(\Delta x D)}{\Delta x^3}.$$

By means of using trigonometrical identities [22], the application of $\mathcal{A}(\mathrm{E})$ to the compacton solution yields

$$\mathcal{A}(\mathrm{E})\,u_c(z) = \frac{2c}{3} + \frac{c}{90}\left(33 + 26\cos\left(\frac{\Delta x}{2}\right) + \cos(\Delta x)\right)\cos\left(\frac{z}{2}\right).$$

Similarly, the application of operators $\mathcal{B}(\mathrm{E})$ and $\mathcal{C}(\mathrm{E})$ to either the compacton solution or its square results in odd functions in z. By means of symmetry considerations the evaluation of Eq. (23) for $\mathcal{P}_1$ yields

$$\begin{aligned}\int_{-2\pi}^{2\pi} u_c(z)^2\,\mathcal{P}_1(u_c(z))\,dz &= -\int_{-2\,\pi}^{2\,\pi} u_c(z)^2\,\mathcal{A}(\mathrm{E})\,\frac{u_c(z) - u_c(z-\zeta)}{\Delta t}\,dz,\\ &= -\frac{16\,\pi c^3}{405\,\Delta t}\left(33 + 26\cos\left(\frac{\Delta x}{2}\right) + \cos(\Delta x)\right)\sin^2\left(\frac{\zeta}{4}\right),\end{aligned} \tag{24}$$

where $\zeta = (c_0 - c)\,\Delta t$. Eq. (24) is the left-hand side of Eq. (12) after multiplication by $27/(80\,\pi c^2)$.

Let us consider the evaluation of Eq. (23) for $\mathcal{P}_2$, cf. Eq. (21), which results in

$$\int_{-2\pi}^{2\pi} u_c(z)^2\,\mathcal{P}_2(u_c(z))\,dz = -\int_{-2\,\pi}^{2\,\pi} u_c(z)^2\left(\mathcal{A}(\mathrm{E})\,\frac{w_c(z)}{\Delta t} - c_0\,\mathcal{B}(\mathrm{E})\,v_c(z)\right)dz - \int_{-2\,\pi}^{2\,\pi} u_c(z)^2\,(\mathcal{B}(\mathrm{E}) + \mathcal{C}(\mathrm{E}))\,(v_c(z))^2\,dz, \tag{25}$$

where, by using Eq. (8),

$$v_c(z) = \frac{u_c(z + \zeta/2) + u_c(z - \zeta/2)}{2} = \frac{2c}{3}\left(1 + \cos\left(\frac{\zeta}{4}\right)\cos\left(\frac{z}{2}\right)\right),$$

and

$$w_c(z) = u_c(z + \zeta/2) - u_c(z - \zeta/2) = -\frac{4c}{3}\sin\left(\frac{\zeta}{4}\right)\sin\left(\frac{z}{2}\right).$$

By means of symmetry considerations,

$$\int_{-2\pi}^{2\pi} u_c(z)^2\,\mathcal{P}_2(u_c(z))\,dz = 0,$$

since operator $\mathcal{A}(\mathrm{E})$ ($\mathcal{B}(\mathrm{E})$ or $\mathcal{C}(\mathrm{E})$) applied to the odd (even) function $w_c(z)$ ($v_c(z)$ or $(v_c(z))^2$) yields an odd result.

References

[1] J.K. Kevorkian, J.D. Cole, Multiple Scale and Singular Perturbation Methods, Springer, New York, 1996.
[2] F.R. Villatoro, J.I. Ramos, On the method of modified equations I: asymptotic analysis of the Euler forward difference method, Appl. Math. Comput. 103 (1999) 111–139.
[3] M. Junk, Z. Yang, Asymptotic analysis of finite difference methods, Appl. Math. Comput. 158 (2004) 267–301.
[4] R.L. Herman, C.J. Knickerbocker, Numerically induced phase shift in the KdV soliton, J. Comput. Phys. 104 (1993) 50–55.
[5] T.R. Marchant, N.F. Smyth, Soliton interaction for the extended Korteweg-de Vries equation, IMA J. Appl. Math. 56 (1996) 157–176.
[6] T.R. Marchant, Numerical solitary wave interaction: the order of the inelastic effect, ANZIAM J. 44 (2002) 95–102.
[7] M. Junk, A. Klar, L.-S. Luo, Asymptotic analysis of the lattice Boltzmann equation, J. Comput. Phys. 210 (2005) 676–704.
[8] P. Rosenau, J.M. Hyman, Compactons: solitons with finite wavelength, Phys. Rev. Lett. 70 (1993) 564–567.
[9] F. Rus, F.R. Villatoro, Self-similar radiation from numerical Rosenau–Hyman compactons, J. Comput. Phys. 227 (2007) 440–454.
[10] A. Pikovsky, P. Rosenau, Phase compactons, Physica D 218 (2006) 56–69.

[11] D.W. McLaughlin, A.C. Scott, Perturbation analysis of fluxon dynamics, Phys. Rev. A 18 (1978) 1652–1680.
[12] G.L. Lamb Jr., Elements of Soliton Theory, John Wiley & Sons, New York, 1980.
[13] J.-C. Fernandez, C. Froeschle, G. Reinisch, Adiabatic perturbations of solitons and shock waves, Phys. Scr. 20 (1979) 545–551.
[14] A. Biswas, S. Konar, Soliton perturbation theory for the compound KdV equation, Int. J. Theor. Phys. 46 (2006) 237–243.
[15] J. de Frutos, M.A. López-Marcos, J.M. Sanz-Serna, A finite difference scheme for the $K(2,2)$ compacton equation, J. Comput. Phys. 120 (1995) 248–252.
[16] M.S. Ismail, T.R. Taha, A numerical study of compactons, Math. Comput. Simul. 47 (1998) 519–530.
[17] F. Rus, F.R. Villatoro, Padé numerical method for the Rosenau–Hyman compacton equation, Math. Comput. Simul. 76 (2007) 188–192.
[18] R.F. Warming, B.J. Hyett, Modified equation approach to stability and accuracy analysis of finite-difference methods, J. Comput. Phys. 14 (1974) 159–179.
[19] G.E. Forsythe, W.R. Wasow, Finite-Difference Methods for Partial Differential Equations, John Wiley & Sons, New York, 1960.
[20] W.F. Ames, Numerical Methods Computation for Partial Differential Equations, Academic Press, Orlando, FL, 1977.
[21] C. Hirsch, Numerical Computation of Internal and External Flows, Fundamentals of Computational Fluid Dynamics, second ed., vol. 1, Elsevier, Amsterdam, 2007.
[22] M. Abramowitz, I.A. Stegun, Handbook of Mathematical Functions with Formulas Graphs and Mathematical Tables, Dover, New York, 1964.